Langmuir

Article

pubs.acs.org/Langmuir

Importance of Hydrophilic Pretreatment in the Hydrothermal Growth of Amorphous Molybdenum Sulfide for Hydrogen Evolution Catalysis

Ranjith Bose,[†] Suresh Kannan Balasingam,[§] Seokhee Shin,[†] Zhenyu Jin,[†] Do Hyun Kwon,[†] Yongseok Jun,*[,‡] and Yo-Sep Min*[,†]

[†]Department of Chemical Engineering and [‡]Department of Materials Chemistry and Engineering, Konkuk University, 120 Neungdong-Ro, Gwangjin-Gu, Seoul 143-701, Korea

[§]Department of Chemistry, School of Natural Science, Ulsan National Institute of Science and Technology (UNIST), Ulsan 689-798, Korea

Supporting Information

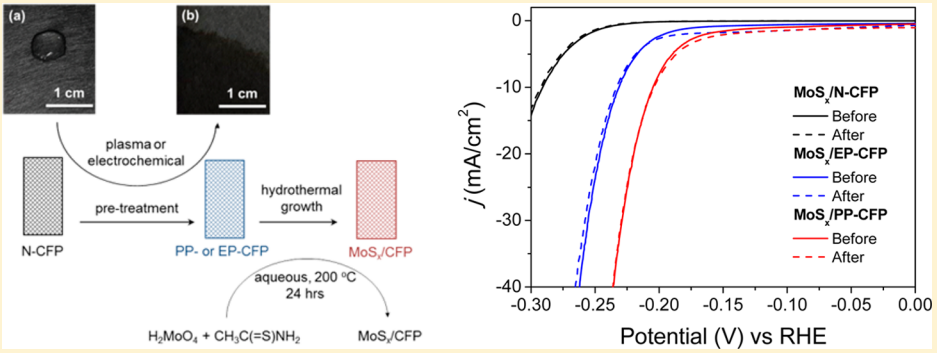

ABSTRACT: Amorphous molybdenum sulfide (MoS_x) has been identified as an excellent catalyst for the hydrogen evolution reaction (HER). It is still a challenge to prepare amorphous MoS_x as a more active and stable catalyst for the HER. Here the amorphous MoS_x catalysts are prepared on carbon fiber paper (CFP) substrates at 200 °C by a simple hydrothermal method using molybdic acid and thioacetamide. Because the CFP is intrinsically hydrophobic due to its graphene-like carbon structure, two kinds of hydrophilic pretreatment methods [plasma pretreatment (PP) and electrochemical pretreatment (EP)] are investigated to convert the hydrophobic surface of the CFP to be hydrophilic prior to the hydrothermal growth of MoS_x. In the HER catalysis, the MoS_x catalysts grown on the pretreated CFPs reach a cathodic current density of 10 mA/cm^2 at a much lower overpotential of 231 mV on the MoS_x/EP-CFP and 205 mV on the MoS_x/PP-CFP, compared to a high overpotential of 290 mV on the MoS_x of the nonpretreated CFP. Turnover frequency per site is also significantly improved when the MoS_x are grown on the pretreated CFPs. However, the Tafel slopes of all amorphous MoS_x catalysts are in the range of 46−50 mV/dec, suggesting the Volmer−Heyrovsky mechanism as a major pathway for the HER. In addition, regardless of the presence or absence of the pretreatment, the hydrothermally grown MoS_x catalyst on CFP exhibits such excellent stability that the degradation of the cathodic current density is negligible after 1000 cycles in a stability test, possibly due to the relatively high growth temperature.

INTRODUCTION

Hydrogen has been considered as a potential source of sustainable and ecofriendly energy. Since hydrogen gas is mostly produced from decomposition of fossil fuels, which accompanies generation of CO_2,[1,2] water splitting has been investigated as an alternate technology for hydrogen production.[3] The electrochemical hydrogen evolution reaction (HER) is one of the significant stages in the water-splitting reaction, where protons and electrons are combined to evolve molecular hydrogen. However, a large thermodynamic overpotential is required to electrochemically split water into hydrogen and oxygen gases. In this regard, highly active catalysts, like platinum-group metals, should be used to lower the overpotential for high thermodynamic efficiency.[4−6] Pt is the best catalyst ever reported for the HER, but it is very expensive due to its low abundance on Earth.[7] On the other hand, non-noble metals like nickel and its alloyed catalysts have shown considerably good activities for the HER in alkaline media. However, they cannot be used in acidic media because of corrosion problems.[8−10] Therefore, it is of great challenge to find cheap, highly active, and stable catalysts for the HER in acidic media.[3,11]

MoS_2 has been considered as a catalyst for the hydrodesulfurization reaction.[12] However, for the HER, bulk

Received: January 19, 2015
Revised: April 15, 2015
Published: April 16, 2015

DOI: 10.1021/acs.langmuir.5b00205
Langmuir 2015, 31, 5220−5227

crystalline MoS_2 shows poor catalytic activity, because the (002) basal planes of MoS_2 are catalytically inert.[13] Recently, nanoparticles of MoS_2 have been identified as an excellent HER catalyst to replace Pt for the electrochemical HER, because edge sites of MoS_2 nanoparticles can mimic the active sites of hydrogenase and nitrogenase to lower the overpotential for the HER.[13−16] Recently, the amorphous phase of MoS_x has also been proposed as an excellent catalyst for the HER.[17−20]

Since the identification of the HER activity on MoS_2,[13,16] several methods have been reported to enhance the HER performance. The main approaches are to increase the number of active sites and to improve the charge transfer through the catalyst. The performance of MoS_2 catalyst is also largely influenced by the supporting substrates such as Au,[13] graphene,[21,22] carbon nanotubes,[11] activated carbon,[16] MoO_3 nanorod arrays,[23] carbon paper,[14] graphitic carbon nitride,[24] TiO_2 nanofibers/particles,[25,26] and graphite.[27] Furthermore, since the catalytic performance can be enhanced by increasing the electrochemically active surface area of MoS_2 catalyst, porous and conducting substrates such as carbon fiber paper (CFP) are preferred as a supporting substrate.[14,28] Chorkendorff and co-workers reported that the electrochemical surface area of the CFP is not as high as expected from its large surface roughness factor (defined as the ratio of real area to geometric area), because of its hydrophobic nature.[28] They proposed pretreating CFP using a piranha solution to improve the wetting of the deposition solution on the CFP and consequently to electrochemically grow MoS_x even on the innermost surface of the CFP. It is also reported that the nature of the surface of the CFP can be converted from hydrophobic to hydrophilic by using O_2 plasma treatment, which helps the wetting of the precursor solution for uniform growth of MoS_x on the surface.[29]

From this point of view, we investigate the effect of hydrophilic pretreatment on the CFP for hydrothermal growth of MoS_x catalyst. Two pretreatment methods are compared to control the hydrophobicity of the CFP: electrochemical pretreatment (EP) and plasma pretreatment (PP). A facile hydrothermal process is used to grow amorphous MoS_x on both pretreated CFPs (PP-CFP and EP-CFP) and nonpretreated CFP (N-CFP) as a control sample. Even though we performed the hydrothermal growth of MoS_x on each CFP under the same conditions, dramatic enhancement of the HER activity was observed on both MoS_x/EP-CFP and MoS_x/PP-CFP in comparison to MoS_x/N-CFP. To the extent of our knowledge, this is the first comparative study on the hydrophilic pretreatment methods for the hydrothermal growth of amorphous MoS_x catalyst using CFP as a supporting substrate.

EXPERIMENTAL SECTION

Plasma Pretreatment (PP). The CFP is hydrophobic in nature due to its graphene-like carbon structure (see Figure 1a). In order to obtain excellent wettability of the precursor solution on the CFP, the hydrophobic surface was converted into a hydrophilic surface by oxygen plasma treatment. The untreated CFP (Toray, TGP-H-120) substrate, which is called N-CFP, was placed in a plasma chamber (Harrick Plasma, PDC-32G) and then activated with an oxygen plasma power of 18 W for 15 min. This modified substrate is called plasma-pretreated carbon fiber paper (PP-CFP).

Electrochemical Pretreatment (EP). The electrochemical treatment was performed in 2 M H_2SO_4 solution using a standard three-electrode setup in which the CFP substrate, silver/silver chloride (Ag/AgCl), and Pt wire were used as a working, reference, and counter electrodes, respectively. For the electrochemical pretreatment, cyclic voltammetry was performed on the CFP in the potential range from +2.545 to −1.955 V versus the reference electrode at a scan rate of 500 mV/s.[30] Subsequently, the CFP was rinsed in deionized water (18 MΩ cm, Millipore) for 1 min and then dried in air. The CFP substrate is called electrochemically pretreated carbon fiber paper (EP-CFP).

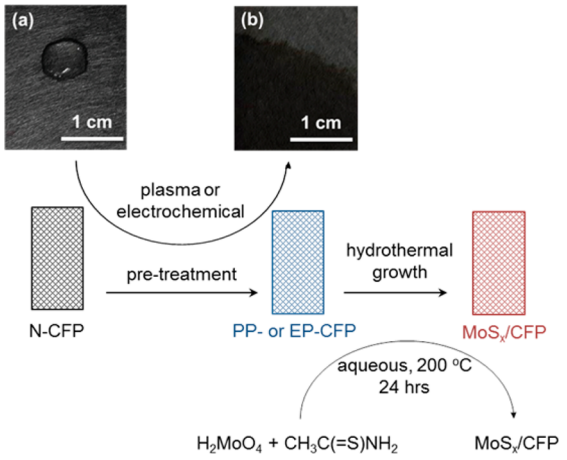

Figure 1. Schematic diagram of the preparation procedure for the amorphous MoS_x catalyst on CFP substrate using a hydrothermal method.

Synthesis of MoS_x on CFP. Molybdic acid (H_2MoO_4) and thioacetamide (CH_3CSNH_2) were purchased from Sigma-Aldrich (ACS grade) and used to prepare the precursor solution for the hydrothermal growth of MoS_x without further purification. In a typical hydrothermal synthesis, 0.121 g (0.75 mmol) of H_2MoO_4 and 0.225 g (3.0 mmol) of CH_3CSNH_2 were weighed and dissolved in 80 mL of deionized water with continuous stirring for a few minutes. The untreated or pretreated CFP substrate was placed into a Teflon-lined stainless steel autoclave and then the as-prepared precursor solution was transferred into the autoclave. The autoclave was heated in a muffle furnace and maintained at 200 °C for 24 h. After the hydrothermal growth, the autoclave was gradually cooled down to room temperature and the MoS_x-coated CFP was taken out. The MoS_x/CFP was washed several times with deionized water and then dried at 40 °C for a few hours.

Characterization. X-ray photoelectron spectroscopic (XPS) spectra were obtained on a PHI 5000 Versaprobe (ULVAC PHI) using monochromatic Al Kα emission. Binding energies were calibrated by using the carbon 1s peak at 284.8 eV. Scanning electron microscopic images were taken with a field emission SEM (Hitachi, S-5500). X-ray diffraction (XRD) measurements for the various samples were recorded using a Philips X'pert Pro MRD X-ray diffractometer with Cu Kα emission. Raman spectra were obtained on a Raman spectrometer (Alpha 500R, WiTec) using 532 nm laser excitation, after calibrating the Raman shift with a reference of Si at 521 cm^{-1}. High-resolution transmission electron microscopic (HR-TEM) images were taken using a transmission electron microscope (FEI, Talos F200X) at an accelerating voltage of 200 kV. Scanning transmission electron microscopic (STEM) images and elemental maps were obtained on the same microscope using the high-angle annular dark field (HAADF) mode. TEM samples were prepared using a focused ion beam equipped scanning electron microscope (FEI, Quanta 3D), after depositing a thin layer of Pt on the samples. The loading amounts of MoS_x on CFP substrates were determined by inductively coupled plasma-optical emission spectroscopy (ICP-OES, Varian 720-ES).

Electrochemical Characterization. The HER measurements were performed in 100 mL of 0.5 M H_2SO_4 electrolyte solution using a standard three-electrode cell with a Bio-Logic potentiostat (SP150). Saturated Hg/Hg_2SO_4, graphite rod, and the MoS_x-coated CFP were used as a reference, counter, and working electrodes, respectively. For the preparation of the working electrode, the geometric area of the MoS_x-coated CFP was defined to be around 1

DOI: 10.1021/acs.langmuir.5b00205
Langmuir 2015, 31, 5220−5227

cm^2 with Kapton tape. The reference electrode was calibrated with respect to the reversible hydrogen electrode (RHE) by using two platinum wires as working and counter electrodes, which gives an electrochemical potential (E) relation between the RHE and counter electrode, $E(RHE) = E(Hg/Hg_2SO_4) + 0.700$ V. Polarization curves for the HER were obtained by linear sweep voltammetry (LSV) beginning at 0.1 V and ending at −0.30 V vs RHE with a scan rate of 5 mV/s. In order to determine series resistance of the electrochemical cell before each LSV experiment, electrochemical impedance measurement was performed at an open circuit potential from 200 kHz to 50 mHz, using an ac amplitude of 25 mV. All polarization curves were corrected for ohmic potential drop (iR) losses using the series resistance (<2Ω, see Figure S1 and Table S1, Supporting Information). To estimate the electrochemically active surface area of the MoS_x-coated CFP, the double-layer capacitance (C_{dl}) of the defined area (1 cm^2) was determined from cyclic voltammograms in a potential range from 0.08 to 0.18 V vs RHE taken at various scan rates (20, 40, 60, 80, and 100 mV/s).

RESULTS AND DISCUSSION

As shown in the schematic diagram in Figure 1, the amorphous MoS_x is directly grown on the pretreated or untreated CFPs from the aqueous solution of molybdic acid and thioacetamide through the simple hydrothermal route.

The CFP used in this work is a porous mat of crystalline carbon fibers of which the diameter is ∼8 μm (Figure 2a), and

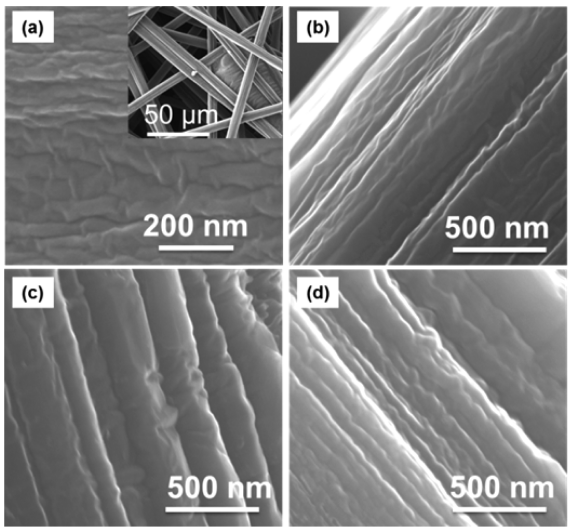

Figure 2. SEM images of (a) bare N-CFP, (b) MoS_x/N-CFP, (c) MoS_x/EP-CFP, and (d) MoS_x/PP-CFP. The inset is a low-magnification image of the bare N-CFP.

the total thickness of the CFP is ∼400 μm. Even though the CFP is hydrophobic, as shown in Figure 1a, after the PP or EP process, the CFP provides a hydrophilic surface for the hydrothermal growth of MoS_x (Figure 1b).

The appearance of MoS_x after hydrothermal growth on the bare substrates of N-, PP-, or EP-CFPs is not significantly different from that before the hydrothermal growth, as shown in Figure 2, due to the thin thickness of the MoS_x. Indeed, when the same hydrothermal method was performed on a bare silicon wafer in order to indirectly determine the MoS_2 thickness, the grown thickness measured by spectroscopic ellipsometry was only several tens of nanometers (data not shown). The thicknesses of MoS_x grown on N-, PP-, and EP-CFPs were also measured to range from 12 to 25 nm by HR-TEM images (Figure S4, Supporting Information). In addition, the loading amounts of MoS_x determined by ICP-OES were not largely different on each CFP (30.2 μg/cm^2 on N-CFP, 30.7 μg/cm^2 on PP-CFP, and 36.1 μg/cm^2 on EP-CFP).

According to the XRD analyses (Figure S2, Supporting Information), the hydrothermally grown MoS_x is amorphous on the CFP, because no characteristic peak of the crystalline MoS_2 is observed but only the graphitic carbon peak is visible. In addition, the HR-TEM images (Figure S4, Supporting Information) of the MoS_x films on N-, PP-, and EP-CFPs clearly show an amorphous phase as characterized by XRD. In Raman spectra, the MoS_x grown on N-CFP and EP-CFP do not show any characteristic Raman modes of MoS_2 (data not shown). However, when investigating many positions over the surface of the MoS_x/PP-CFP, two distinctive E^1_{2g} (in-plane) and A_{1g} (out-of-plane) modes of MoS_2 are very occasionally observed with a small intensity, as shown in Figure S3 (Supporting Information). Recently, Jin et al. also reported that MoS_2 thin films grown by atomic layer deposition showed the characteristic Raman modes despite the amorphous phase.[31]

The chemical states of Mo and S were investigated on the amorphous MoS_x catalysts grown on N-, EP-, and PP-CFPs by XPS. The binding energies were calibrated by using the carbon 1s peak at 284.8 eV. As shown in Figure 3, the doublets of Mo for all samples are clearly resolved at 229.1−229.2 eV for the $3d_{5/2}$ peaks and 232.3−232.4 eV for the $3d_{3/2}$ peaks (see Table S2 of the Supporting Information for the XPS peak positions for each sample), indicating the oxidation state of Mo^{4+}.[17,32−34] However, the 2p doublets of S atoms are not clearly resolved due to the amorphous nature of MoS_x. The stoichiometric ratios of S to Mo, determined from XPS peak intensities, are around 3.8, 3.5, and 2.9 on the N-, EP-, and PP-CFP, respectively. As shown in Figures S2 and S4 (Supporting Information), MoS_x on CFPs has the amorphous phase after hydrothermal growth at 200 °C. The reason for the formation of amorphous phase at 200 °C may be the excess sulfur present in the MoS_x which hinders the formation of the crystalline phase. However, after removing the surface species by Ar^+ ion bombardment, the S/Mo ratios are reduced to 3.0, 2.6, and 2.1 on the N-, EP-, and PP-CFP, respectively. This may be due to a preferential sputtering of S to Mo during the bombardment. The high content of S reveals that the hydrothermally grown MoS_x resembles MoS_3 rather than MoS_2.[19] It is well-known that amorphous MoS_3, of which the formal charge state is $Mo^{4+}(S^{2-})(S_2^{2-})$, can be used as a HER catalyst, because the catalytically inactive S_2^{2-} can be reduced to the active S^{2-} by applying a cathodic potential during the HER process.[17,19,35]

In order to determine the relative ratio of S^{2-}/S_2^{2-} in the MoS_x catalyst, the 2p spectra were deconvoluted to two doublets of S^{2-} and S_2^{2} in Figure 3.[17,32,33] The curve fitting was performed with two constraints, the intensity ratio (1:2) and the binding energy difference (1.18 eV) of the doublet (see Table S2 of the Supporting Information for the deconvoluted peak positions of each sample). It is well-known that the doublet of S_2^{2-} appears at a higher binding energy than that of S^{2-}, as shown in Figure 3.[32] The ratios of S^{2-} to S_2^{2-} are evaluated to be ∼0.33 (MoS_x/N-CFP), ∼ 0.64 (MoS_x/EP-CFP), and ∼0.65 (MoS_x/PP-CFP) from the peak intensities. It should be noted that the contribution of MoS_2 to the amorphous phase becomes larger as the S^{2-}/S_2^{2-} ratio increases. Therefore, it is believed that the EP and PP pretreatments are significantly effective in increasing the contribution of the amorphous MoS_2 phase to the catalyst. In addition, note that MoS_x/EP-CFP and MoS_x/PP-CFP have

DOI: 10.1021/acs.langmuir.5b00205
Langmuir 2015, 31, 5220−5227

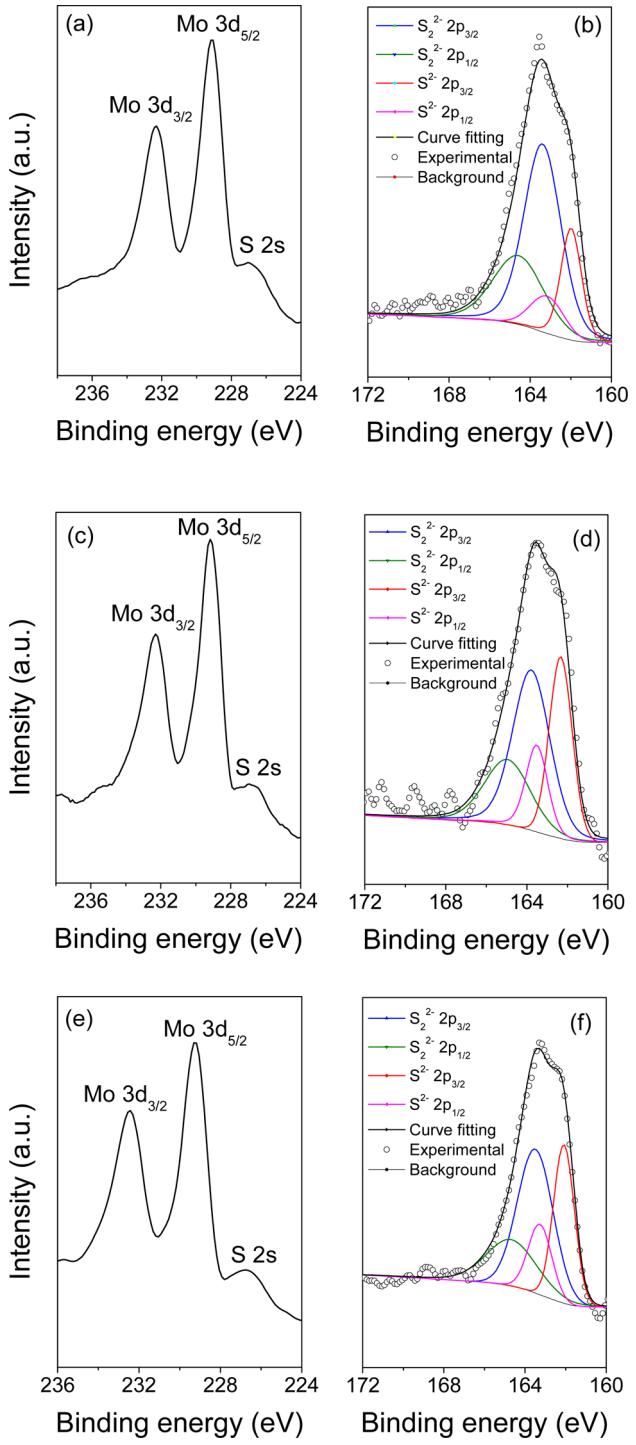

Figure 3. XPS spectra of amorphous MoS_x: (a) Mo 3d and (b) S 2p on MoS_x/N-CFP, (c) Mo 3d and (d) S 2p on MoS_x/EP-CFP, and (e) Mo 3d and (f) S 2p on MoS_x/PP-CFP.

similar S^{2-}/S_2^{2-} ratios, even though the S/Mo ratio of the former is significantly higher than that of the latter. This reveals that the amorphous phase of MoS_2 may be more incorporated into the MoS_x/PP-CFP compared to the MoS_x/EP-CFP. This is consistent with the Raman observation, in which the characteristic E^1_{2g} and A_{1g} modes are occasionally observed only on the MoS_x/PP-CFP, while the other two samples do not show any peak.

We investigated the electrocatalytic HER activity of each bare CFP and MoS_x-grown CFP in 0.5 M H_2SO_4 solution. As shown in the polarization curves (dotted lines) of Figure 4, all bare

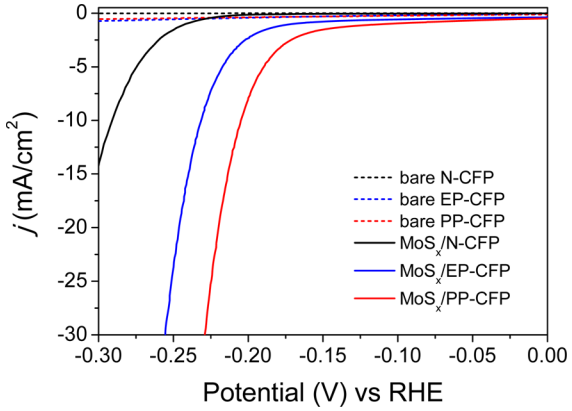

Figure 4. HER polarization curves of the bare CFPs and MoS_x-grown CFPs.

CFPs are catalytically inert for the HER, regardless of the hydrophilic pretreatment. However, the MoS_x-grown N-, EP-, and PP-CFPs show excellent HER activities. It should be noted that a larger cathodic current density (j) at a lower overpotential (μ) indicates noticeable hydrogen evolution with low energy consumption. The overpotentials required to reach a current density of 10 mA/cm^2 are 290, 231, and 205 mV in the MoS_x-grown N-, EP-, and PP-CFP, respectively, which are similar to the previous reports.[14,36−39] The polarization curves also suggest the superior HER activities of the amorphous MoS_x grown on the hydrophilic pretreated CFPs in comparison to the MoS_x/N-CFP without any pretreatment. In addition, the cathodic current density of MoS_x/PP-CFP is significantly higher than that of MoS_x/EP-CFP in the whole potential region. At the overpotential of 200 mV, the current density of the MoS_x/PP-CFP is 8.13 mA/cm^2, which is 3 and 50 times higher than those of MoS_x/EP-CFP (2.36 mA/cm^2) and MoS_x/N-CFP (0.16 mA/cm^2), respectively. Such a high current density at a low overpotential reveals that the PP process is more effective than the EP one to enhance the catalytic activity of amorphous MoS_x prepared by hydrothermal growth.

In the Tafel plot, in which the overpotential is plotted against the logarithm of the cathodic current density (Figure 5), the figures of merit for the electrocatalytic activity of the MoS_x are obtained from the slope (Tafel slope, b) and intercept (geometric exchange current density, j_0). The linear portion of the Tafel plot is fitted to the Tafel equation: $\eta = a + b \log j$. In general, a smaller Tafel slope is advantageous for practical catalytic applications, because the HER can be more rapidly accelerated by increasing the overpotential. As summarized in Table 1, the Tafel slopes of the amorphous MoS_x ranged from 46 to 50 mV/dec, which is similar to the previous reports. Depending on the preparation methods, substrates, and composition of the amorphous MoS_x, they reported Tafel slopes ranging from 35 to 65 mV/dec by chemical reduction (35 mV/dec),[40] electrochemical deposition (40 mV/dec),[17,35] atomic layer deposition (47 mV/dec),[41] and wet chemical synthesis (60 mV/dec).[19] According to the classical theory on HER kinetics, the Tafel slopes ranging from 46 to 50 mV/dec reveal that the HER on amorphous MoS_x occurs via the

DOI: 10.1021/acs.langmuir.5b00205
Langmuir 2015, 31, 5220−5227

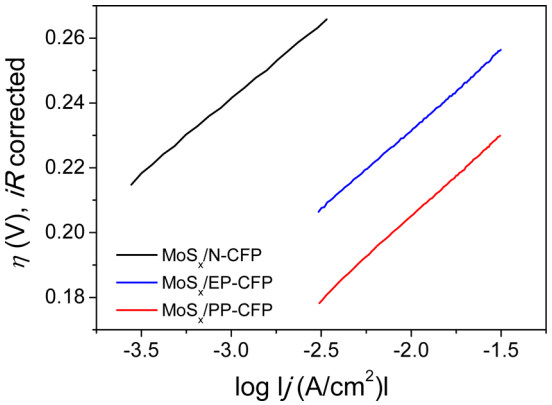

Figure 5. Tafel plots of MoS_x/N-CFP, MoS_x/EP-CFP, and MoS_x/PP-CFP.

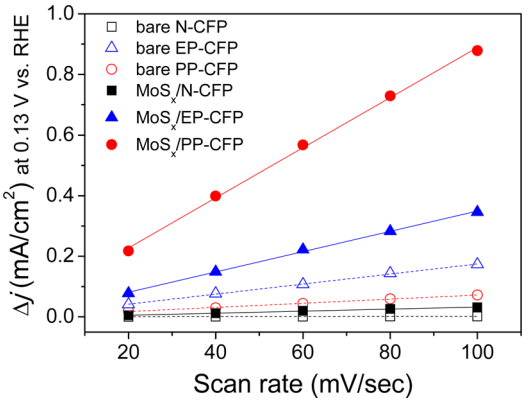

Figure 6. Differences of anodic and cathodic current densities ($\Delta j = j_a - j_c$) at 0.13 V vs RHE plotted against scan rate.

Table 1. Figures of Merit for Electrocatalytic Activities of MoS_x Catalysts

catalyst	Tafel slope (mV/dec)	$j_0 = i_0/A_g$ (μA/cm^2)	$j_0^* = i_0/A_e$ (μA/cm^2)
MoS_x/N-CFP	46	0.006	0.002
MoS_x/EP-CFP	49	0.178	0.006
MoS_x/PP-CFP	50	0.863	0.013

Volmer–Heyrovsky mechanism, in which the fast Volmer reaction (discharge step) is followed by the rate-determining Heyrovsky reaction (electrochemical desorption step).[13,18,23,41,42] Considering the uncertainty in choosing the linear portions of the Tafel plots, there may be no significant difference among the three samples. Therefore, we believe that the hydrophilic pretreatment process may not result in any change of the HER mechanism.

The exchange current density (j_0), a measure of the rate of electrochemical reaction at equilibrium (i.e., $\eta = 0$), is one of the widely used metrics to evaluate the HER activity. The j_0 values of MoS_x/EP-CFP and MoS_x/PP-CFPs are 30 and 145 times higher than that of MoS_x/N-CFP. It should be noted that the exchange current density generally depends on the Gibbs free energy of the hydrogen adsorption (ΔG_{H^*}) in the volcano curve of the HER catalysts.[5,43] When the $|\Delta G_{H^*}|$ value approaches zero, the j_0 value is maximized at the top of the volcano curve. Therefore, it is possible that an increase of the exchange current density as large as an order of magnitude might originate from the smaller $|\Delta G_{H^*}|$ values for the adsorption of H^+ on the MoS_x/EP-CFP and MoS_x/PP-CFPs, comparing to the adsorption on the MoS_x/N-CFP. Another origin of the large increase of the j_0 value may be the large difference of electrochemically active areas (A_e) of MoS_x grown on N-, EP-, and PP-CFPs. Even though the geometric area (A_g) of each catalyst is identically defined to be $A_g = 1$ cm^2, the A_e values may differ depending on the pretreatment process (vide infra).

In order to estimate the A_e values of each catalyst, we determined the double-layer capacitance (C_{dl}) of each CFP before and after the hydrothermal growth by using cyclic voltammograms (CVs, Figure S6, Supporting Information). The CVs were obtained in a potential range of 0.08–0.18 V vs RHE with different scan rates (υ = 20, 40, 60, 80, and 100 mV/s).[19] Because there was no obvious Faradic current in the region, the potential range was chosen for the capacitance measurements. Figure 6 shows the differences ($\Delta j = j_a - j_c$) of anodic and cathodic current densities at the middle (0.13 V vs RHE) of the CVs as a function of the scan rate. Because half of the Δj is the non-Faradic capacitive current density for the electrical double layer charging, the double-layer capacitance can be expressed as $C_{dl} = \Delta j/2\upsilon$. Therefore, the slope of each plot in Figure 6 is equal to $2C_{dl}$. By linearly fitting the data, in which R^2 values are ranged from 0.995 to 0.998, the C_{dl} values of N-, EP-, and PP-CFPs are 7.9, 830, and 343 μF/cm^2, respectively, before the hydrothermal growth. Compared to N-CFP, both EP- and PP-CFP exhibit much higher C_{dl} values due to the effect of the hydrophilic pretreatment. In addition, the EP process may be more effective than the PP process in terms of activating the surface of the CFP to achieve a higher A_e, because C_{dl} is directly proportional to A_e.

After the hydrothermal growth of MoS_x on each bare CFP, the C_{dl} values of MoS_x/N-CFP, MoS_x/EP-CFP, and MoS_x/PP-CFP are 170, 1675, and 4130 μF/cm^2, respectively. For all samples, the C_{dl} values largely increase due to the presence of MoS_x grown on the bare CFPs. Several groups reported that the C_{dl} of MoS_2 is ~60 μF/cm^2 in a form of flat thin film.[19,44] Therefore, the A_e values of MoS_x/N-CFP, MoS_x/EP-CFP, and MoS_x/PP-CFP are 2.8, 27.9, and 68.8 times larger than the geometric area (A_g = 1 cm^2 for all samples), respectively. Furthermore, although the EP process is more efficient than the PP process, as mentioned above, the A_e value of the MoS_x/PP-CFP is 2.5 times larger than that of MoS_x/EP-CFP. This reveals that the surface functional groups formed by the PP process are more reactive to the hydrothermal growth of MoS_x than those formed by the EP process.

Considering the large differences between the A_g and A_e values for each sample, the geometrically defined exchange current densities ($j_0 = i_0/A_g$, where i_0 is the exchange current) are exaggerated. Therefore, we modify the j_0 value to an electrochemically effective exchange current density ($j_0^* = i_0/A_e$). The j_0^* values of each catalyst are summarized in Table 1. According to the previous reports,[13,20,41] the exchange current density of molybdenum sulfide grown on flat substrates is broadly ranged from 10^{-8} to 10^{-6} A/cm^2. The j_0^* values of MoS_x/N-CFP and MoS_x/EP-CFP are 0.002 and 0.006 μA/cm^2, and these values are out of the range of the previous report. However, the j_0^* value of 0.013 μA/cm^2 well agrees with the previous report, suggesting that MoS_x is more uniformly grown on the PP-CFP, achieving a higher A_e, in comparison to the EP-CFP and N-CFP (vide supra).

The turnover frequency (TOF) per site, which is the number of H_2 evolved on an active site for a unit time (e.g., 1 s), is an

DOI: 10.1021/acs.langmuir.5b00205
Langmuir 2015, 31, 5220–5227

essential parameter to estimate inherent catalytic activity.[45] Even though a value of TOF is only approximate because of the uncertainty in counting the number of active sites in an unit geometric area (N), it can immediately be used to compare the inherent HER activity. The per-site TOF can be calculated by the equation TOF = jN_A/nFN, where n is the stoichiometric number of electrons consumed in the electrode reaction (n = 2 for the HER), and N_A and F are Avogadro's number and the Faraday constant, respectively. By using the number of active sites (N = 1.164 × 10^{15}/cm^2) in the flat surface of MoS_2 and the A_e values of each sample,[19] the N values of MoS_x/N-CFP, MoS_x/EP-CFP, and MoS_x/PP-CFP are calculated as 3.26 × 10^{15}, 3.25 × 10^{16}, and 8.01 × 10^{16}/cm^2, respectively. Figure 7

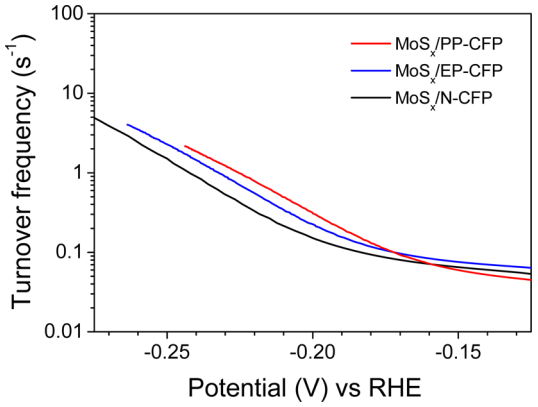

Figure 7. Turnover frequencies of MoS_x/N-CFP, MoS_x/EP-CFP, and MoS_x/PP-CFP.

shows the TOF (per active site) of amorphous MoS_x grown on nonpretreated and pretreated CFPs. The TOFs are drawn within the Tafel region in order to guarantee that the HER is controlled by electrode kinetics without any other effect (e.g., mass transfer). The TOFs at high overpotentials of MoS_x/EP-CFP and MoS_x/PP-CFP are significantly higher than that of MoS_x/N-CFP. The TOF values at the overpotential of 0.2 V are 0.15, 0.23, and 0.32 H_2/s for MoS_x/N-CFP, MoS_x/EP-CFP, and MoS_x/PP-CFP, respectively. The most active MoS_x/PP-CFP turns over the catalytic cycle with TOFs of 0.8 H_2/s at 0.22 V and 2 H_2/s at 0.24 V. These TOF values well agree with the previously reported values for amorphous MoS_x: for the wet chemical synthesis, 0.3 H_2/s at 0.2 V; for the electrochemical deposition, 0.8 H_2/s at 0.22 V and 2 H_2/s at 0.24 V.[17,19] Therefore, it is believed that the per-site catalytic activity of the hydrothermally grown MoS_x may be similar to that of the other amorphous MoS_x prepared by the wet chemical synthesis and electrochemical deposition. The significantly higher TOF values of MoS_x/EP-CFP and MoS_x/PP-CFP may be related to the chemical state of sulfur, as inferred from the higher ratio of S^{2-}/S_2^{2-} in MoS_x/EP-CFP (~0.64) and MoS_x/PP-CFP (~0.65) compared to MoS_x/N-CFP (~0.33). Indeed, the amorphous MoS_2 grown by atomic layer deposition, of which the ratio of S^{2-}/S_2^{2-} is around 6.4, shows a high TOF of 1.45 H_2/s at 0.2 V. In addition, the origin of the excellent hydrogen evolution on the MoS_x/PP-CFP is not only the high TOF but also the abundant active site density due to the hydrophilic PP process.

Stability is also of important concern for long-term operation of the catalyst. The stability of each catalyst was tested by repeating a cyclic potential scan in the range from +0.2 to −0.2 V vs RHE with a scan rate of 100 mV/s. As shown in Figure 8, changes of the cathodic current densities are negligible after

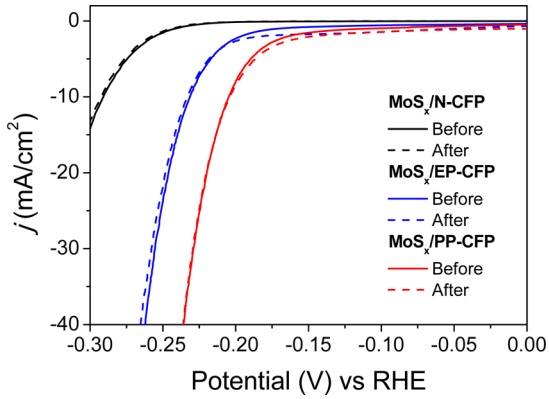

Figure 8. Polarization curves of MoS_x catalysts before and after 1000 CV cycles between −0.2 and +0.2 V.

1000 cycles for all catalysts. The overpotentials for a current density of 10 mA/cm^2 are 292, 233, and 204 mV for MoS_x/N-CFP, MoS_x/EP-CFP, and MoS_x/PP-CFP, respectively, after the stability test. Therefore, the overpotential differences before and after the 1000 cycles are only 2 mV for both MoS_x/N-CFP and MoS_x/EP-CFP and 1 mV for MoS_x/PP-CFP. The high stability may be due to the relatively high growth temperature of 200 °C.[20] The Tafel slopes also slightly increase to 47, 51, and 55 mV/dec for MoS_x/N-CFP, MoS_x/EP-CFP, and MoS_x/PP-CFP, respectively (Figure S7, Supporting Information). This suggests that the HER mechanism is not significantly changed by the potential cycling.

CONCLUSIONS

Amorphous MoS_x HER catalysts with high performance and long-term stability are prepared on the supporting substrate of CFP via facile hydrothermal growth using molybdic acid and thioacetamide. Because of the hydrophobic nature of the CFP, the HER performance, such as exchange current density and cathodic current density at a given overpotential, is dramatically enhanced by activating the CFP by the hydrophilic EP or PP process prior to the hydrothermal growth. This mainly originated from the large electrochemically active surface area of MoS_x on the pretreated CFP. In addition, the per-site TOF is also significantly improved when MoS_x is grown on the hydrophilic pretreated CFP. This may be related to the chemical state of sulfur, as inferred from the higher ratio of S^{2-}/S_2^{2-} in the MoS_x grown on the EP- or PP-CFPs. However, regardless of the presence of the hydrophilic pretreatment, the Tafel slopes are not significantly different, suggesting that the HER catalysis follows the Volmer−Heyrovsky mechanism on all catalysts. Furthermore, all samples exhibit such excellent stability that the degradation of the cathodic current density is negligible after 1000 cycles of the HER experiments, possibly due to the relatively high growth temperature of 200 °C.

ASSOCIATED CONTENT

Supporting Information

Ohmic potential drop correction, XRD patterns, Raman spectrum, HR-TEM and elemental mapping images, deconvoluted XPS data, electrochemical capacitance measurement data, and Tafel plots after the stability test. The Supporting

DOI: 10.1021/acs.langmuir.5b00205
Langmuir 2015, 31, 5220−5227

Information is available free of charge on the ACS Publications website at DOI: 10.1021/acs.langmuir.5b00205.

AUTHOR INFORMATION

Corresponding Authors

*Y.J. e-mail: yjun@konkuk.ac.kr.
*Y.S.M. e-mail: ysmin@konkuk.ac.kr.

Author Contributions

R.B and S.K.B. contributed equally to this work.

Notes

The authors declare no competing financial interest.

ACKNOWLEDGMENTS

This work was supported by Basic Science Research Program through the National Research Foundation of Korea, which is funded by the Ministry of Education (NRF: 2014R1A1A2055812). This research was also partially supported by the Korea Evaluation Institute of Industrial Technology (KEIT10050509).

REFERENCES

(1) Turner, J. A. Sustainable Hydrogen Production. *Science* **2004**, *305* (5686), 972−974.
(2) Armor, J. N. Catalysis and the Hydrogen Economy. *Catal. Lett.* **2005**, *101* (3−4), 131−135.
(3) Walter, M. G.; Warren, E. L.; Mckone, J. R.; Boettcher, S. W.; Mi, Q. X.; Santori, E. A.; Lewis, N. S. Solar Water Splitting Cells. *Chem. Rev.* **2010**, *110*, 6446−6473.
(4) Conway, B. E.; Tilak, B. V. Interfacial Processes Involving Electrocatalytic Evolution and Oxidation of H_2, and the Role of Chemisorbed H. *Electrochim. Acta* **2002**, *47*, 3571−3594.
(5) Greeley, J.; Jaramillo, T. F.; Bonde, J.; Chorkendorff, I. B.; Norskov, J. K. Computational High-Throughput Screening of Electrocatalytic Materials for Hydrogen Evolution. *Nat. Mater.* **2006**, *5* (11), 909−913.
(6) Li, X.; Yu, J.; Low, J.; Fang, Y. B.; Xiao, J.; Chen, X. Engineering Heterogeneous Semiconductors for Solar Water Splitting. *J. Mater. Chem. A* **2015**, *3*, 2485−2534.
(7) Le Goff, A.; Artero, V.; Jousselme, B.; Tran, P. D.; Guillet, N.; Metaye, R.; Fihri, A.; Palacin, S.; Fontecave, M. From Hydrogenases to Noble Metal-Free Catalytic Nanomaterials for H_2 Production and Uptake. *Science* **2009**, *326*, 1384−7.
(8) Choquette, Y.; Brossard, L.; Lasia, A.; Menard, H. Investigation of Hydrogen Evolution on Raney-Nickel Composite-Coated Electrodes. *Electrochim. Acta* **1990**, *35*, 1251−1256.
(9) Lačnjevac, U. Č.; Jović, B. M.; Jović, V. D.; Krstajić, N. V. Determination of Kinetic Parameters for the Hydrogen Evolution Reaction on the Electrodeposited Ni−MoO_2 Composite Coating in Alkaline Solution. *J. Electroanal. Chem.* **2012**, *677*−*680*, 31−40.
(10) McKone, J. R.; Sadtler, B. F.; Werlang, C. A.; Lewis, N. S.; Gray, H. B. Ni−Mo Nanopowders for Efficient Electrochemical Hydrogen Evolution. *ACS Catal.* **2013**, *3* (2), 166−169.
(11) Laursen, A. B.; Kegnæs, S.; Dahl, S.; Chorkendorff, I. Molybdenum Sulfides—Efficient and Viable Materials for Electro- and Photoelectrocatalytic Hydrogen Evolution. *Energy Environ. Sci.* **2012**, *5* (2), 5577−5591.
(12) Chianelli, R.; Siadati, M.; Perez de la Rosa, M.; Berhault, G.; Wilcoxon, J.; Bearden, R.; Abrams, B. Catalytic Properties of Single Layers of Transition Metal Sulfide Catalytic Materials. *Catal. Rev.* **2006**, *48*, 1−41.
(13) Jaramillo, T. F.; Jorgensen, K. P.; Bonde, J.; Nielsen, J. H.; Horch, S.; Chorkendorff, I. Identification of Active Edge Sites for Electrochemical H_2 Evolution from MoS_2 Nanocatalysts. *Science* **2007**, *317* (5834), 100−102.
(14) Bonde, J.; Moses, P. G.; Jaramillo, T. F.; Norskov, J. K.; Chorkendorff, I. Hydrogen Evolution on Nano-Particulate Transition Metal Sulfides. *Faraday Discuss.* **2008**, *140*, 219−231.
(15) Wang, T.; Gao, D.; Zhuo, J.; Zhu, Z.; Papakonstantinou, P.; Li, Y.; Li, M. Size-Dependent Enhancement of Electrocatalytic Oxygen-Reduction and Hydrogen-Evolution Performance of MoS_2 Particles. *Chem.—Eur. J.* **2013**, *19*, 11939−11948.
(16) Hinnemann, B.; Moses, P. G.; Bonde, J.; Jorgensen, K. P.; Nielsen, J. H.; Horch, S.; Chorkendroff, I.; Norskov, J. K. Biomimetic Hydrogen Evolution: MoS_2 Nanoparticles as Catalyst for Hydrogen Evolution. *J. Am. Chem. Soc.* **2005**, *127*, 5308−5309.
(17) Merki, D.; Fierro, S.; Vrubel, H.; Hu, X. L. Amorphous Molybdenum Sulfide Films as Catalysts for Electrochemical Hydrogen Production in Water. *Chem. Sci.* **2011**, *2*, 1262−1267.
(18) Merki, D.; Vrubel, H.; Rovelli, L.; Fierro, S.; Hu, X. Fe, Co, and Ni Ions Promote the Catalytic Activity of Amorphous Molybdenum Sulfide Films for Hydrogen Evolution. *Chem. Sci.* **2012**, *3*, 2515−2525.
(19) Benck, J. D.; Chen, Z.; Kuritzky, L. Y.; Forman, A. J.; Jaramillo, T. F. Amorphous Molybdenum Sulfide Catalysts for Electrochemical Hydrogen Production: Insights into the Origin of Their Catalytic Activity. *ACS Catal.* **2012**, *2*, 1916−1923.
(20) Li, Y.; Yu, Y.; Huang, Y.; Nielsen, R. A.; Goddard, W. A.; Li, Y.; Cao, L. Engineering the Composition and Crystallinity of Molybdenum Sulfide for High-Performance Electrocatalytic Hydrogen Evolution. *ACS Catal.* **2015**, *5*, 448.
(21) Li, Y.; Wang, H.; Xie, L.; Liang, Y.; Hong, G.; Dai, H. MoS_2 Nanoparticles Grown on Graphene: An Advanced Catalyst for the Hydrogen Evolution Reaction. *J. Am. Chem. Soc.* **2011**, *133*, 7296−7299.
(22) Yan, Y.; Xia, B.; Qi, X.; Wang, H.; Xu, R.; Wang, J. Y.; Zhang, H.; Wang, X. Nano-Tungsten Carbide Decorated Graphene as Co-Catalysts for Enhanced Hydrogen Evolution on Molybdenum Disulfide. *Chem. Commun.* **2013**, *49*, 4884−4886.
(23) Chen, Z.; Cummins, D.; Reinecke, B. N.; Clark, E.; Sunkara, M. K.; Jaramillo, T. F. Core−Shell MoO_3−MoS_2 Nanowires for Hydrogen Evolution: A Functional Design for Electrocatalytic Materials. *Nano Lett.* **2011**, *11*, 4168−4175.
(24) Ge, L.; Han, C.; Xiao, X.; Guo, L. Synthesis and Characterization of Composite Visible Light Active Photocatalysts MoS_2-g-C_3N_4 with Enhanced Hydrogen Evolution Activity. *Int. J. Hydrogen Energy* **2013**, *38*, 6960−6969.
(25) Liu, C.; Wang, L.; Tang, Y.; Luo, S.; Liu, Y.; Zhang, S.; Zeng, Y.; Xu, Y. Vertical Single or Few Layer MoS_2 Nanosheets Rooting into TiO_2 Nanofibers for Highly Efficient Photocatalytic Hydrogen Evolution. *Appl. Catal. B* **2015**, *164*, 1−9.
(26) Xiang, Q.; Yu, J.; Jaroniec, M. Synergetic Effect of MoS_2 and Graphene As Cocatalysts for Enhanced Photocatalytic H_2 Production Activity of TiO_2 Nanoparticles. *J. Am. Chem. Soc.* **2012**, *134*, 6575−6578.
(27) Jaramillo, T. F.; Bonde, J.; Zhang, J.; Ooi, B. L.; Andersson, K.; Ulstrup, J.; Chorkendorff, I. Hydrogen Evolution on Supported Incomplete Cubane-type $[Mo_3S_4]^{4+}$ Electrocatalysts. *J. Phys. Chem. C* **2008**, *112*, 17492−17498.
(28) Laursen, A. B.; Vesborg, P.; Chorkendorff, I. A High-Porosity Carbon Molybdenum Sulphide Composite with Enhanced Electrochemical Hydrogen Evolution and Stability. *Chem. Commun.* **2013**, *49*, 4965−4967.
(29) Wang, H.; Kong, D.; Sun, J.; Hymel, T. M.; Cui, Y. Electrochemical Tuning of MoS_2 Nanoparticles on Three-Dimensional Substrate for Efficient Hydrogen Evolution. *ACS Nano* **2014**, *8*, 4940−4947.
(30) Dong, S.; Wang, B. Electrochemical Preparation of Microelectrodes Modified with Non-Stoichiometric Mixed-Valent Molybdenum Oxides. *J. Electroanal. Chem.* **1994**, *370*, 141−143.
(31) Jin, Z.; Shin, S.; Kwon, D. H.; Han, S. J.; Min, Y. S. Novel Chemical Route for Atomic Layer Deposition of MoS_2 Thin Film on SiO_2/Si Substrate. *Nanoscale* **2014**, *6*, 14453−14458.
(32) Weber, Th.; Muijsers, J. C.; Niemantsverdriet, J. W. Structure of Amorphous MoS_3. *J. Phys. Chem.* **1995**, *99*, 9194−9200.

DOI: 10.1021/acs.langmuir.5b00205
Langmuir 2015, 31, 5220−5227

(33) Muijsers, J. C.; Weber, Th.; van Hardeveld, R. M.; Zandbergen, H. W.; Niemantsverdriet, J. W. Sulfidation study of Molybdenum oxide using $MoO_3/SiO_2/Si(100)$ Model Catalysts and Mo^{IV}−Sulfur Cluster Compounds. *J. Catal.* **1995**, *157*, 698−705.
(34) Xie, J.; Zhang, H.; Li, S.; Wang, R.; Sun, X.; Zhou, M.; Zhou, J.; Lou, W.; Xie, Y. Defect-Rich MoS_2 Ultrathin Nanosheets with Additional Active Edge Sites for Enhanced Electrocatalytic Hydrogen Evolution. *Adv. Mater.* **2013**, *25* (40), 5807−5813.
(35) Vrubel, H.; Hu, X. Growth and Activation of an Amorphous Molybdenum Sulfide Hydrogen Evolving Catalyst. *ACS Catal.* **2013**, *3*, 2002−2011.
(36) Deng, J.; Yuan, W.; Ren, P.; Wang, Y.; Deng, D.; Zhang, Z.; Bao, X. High-Performance Hydrogen Evolution Electrocatalysis by Layer-Controlled MoS_2 Nanosheets. *RSC Adv.* **2014**, *4*, 34733−34738.
(37) Deng, J.; Ren, P.; Deng, D.; Yu, L.; Yang, F.; Bao, X. Highly Active and Durable Non-Precious-Metal Catalysts Encapsulated in Carbon Nanotubes for Hydrogen Evolution Reaction. *Energy Environ. Sci.* **2014**, *7*, 1919−1923.
(38) Youn, D. H.; Han, S.; Kim, J. Y.; Kim, J. Y.; Park, H.; Choi, S. H.; Lee, J. S. Highly Active and Stable Hydrogen Evolution Electrocatalysts Based on Molybdenum Compounds on Carbon Nanotube−Graphene Hybrid Support. *ACS Nano* **2014**, *8*, 5164−5173.
(39) Ji, S.; Yang, Z.; Zhang, C.; Liu, Z.; Tjiu, W. W.; Phang, I. Y.; Zhang, Z.; Pan, J.; Liu, T. Exfoliated MoS_2 Nanosheets as Efficient Catalysts for Electrochemical Hydrogen Evolution. *Electrochim. Acta* **2013**, *109*, 269−275.
(40) Vrubel, H.; Moehl, T.; Gratzel, M.; Hu, X. Revealing and Accelerating Slow Electron Transport in Amorphous Molybdenum Sulfide Particles for Hydrogen Evolution Reaction. *Chem. Commun.* **2013**, *49*, 8985−8987.
(41) Shin, S.; Jin, Z.; Kwon, D. H.; Bose, R.; Min, Y.-S. High Turnover Frequency of Hydrogen Evolution Reaction on Amorphous MoS_2 Thin Film Directly Grown by Atomic Layer Deposition. *Langmuir* **2015**, *31*, 1196−1202.
(42) Raybaud, P.; Hafner, J.; Kresse, G.; Kasztelan, S.; Toulhoat, H. Ab Initio Study of the H_2−H_2S/MoS_2 Gas−Solid Interface: The Nature of the Catalytically Active Sites. *J. Catal.* **2000**, *189*, 129−146.
(43) Norskov, J. K.; Bligaard, T.; Logadottir, A.; Kitchin, J. R.; Chen, J. G.; Pandelov, S.; Stimming, U. Trends in the Exchange Current for Hydrogen Evolution. *J. Electrochem. Soc.* **2005**, *152*, J23−J26.
(44) Yu, Y.; Huang, S. Y.; Li, Y.; Steinmann, S.; Yang, W.; Cao, L. Layer-Dependent Electrocatalysis of MoS_2 for Hydrogen Evolution. *Nano Lett.* **2014**, *14*, 553−558.
(45) Boudart, M. Turnover Rates in Heterogeneous Catalysis. *Chem. Rev.* **1995**, *95*, 661−666.

DOI: 10.1021/acs.langmuir.5b00205
Langmuir 2015, 31, 5220−5227

SUPPORTING INFORMATION

Importance of Hydrophilic Pretreatment in Hydrothermal Growth of Amorphous Molybdenum Sulfide for Hydrogen Evolution Catalysis

Ranjith Bose,[1,†] Suresh Kannan Balasingam,[2,†] Seokhee Shin,[1] Zhenyu Jin,[1] Do Hyun Kwon,[1] Yongseok Jun[3,*], and Yo-Sep Min[1,*]

[1]Department of Chemical Engineering, Konkuk University, 120 Neungdong-Ro, Gwangjin-Gu, Seoul 143-701, Korea

[2]Department of Chemistry, School of Natural science, Ulsan National Institute of Science and Technology (UNIST), Ulsan 689-798, Korea

[3]Department of Materials chemistry and Engineering, Konkuk University, 120 Neungdong-Ro, Gwangjin-Gu, Seoul, 143-701, Korea

[†] These authors equally contributed to this work.

* E-mail: ysmin@konkuk.ac.kr; yjun@konkuk.ac.kr

Ohmic potential drop (*iR*) correction

The ohmic drop correction was performed with a series resistance (R_s) determined by electrochemical impedance measurement. The electrochemical impedance spectroscopy was performed from 200 kHz to 50 mHz at an open circuit voltage of 25 mV. The intercept of the semicircle on the real axis was assigned to the ohmic series resistance (Table S1). The *iR* correction to data with the series resistance is done by the equation of $\eta_{corr} = \eta_{exp} - iR$.

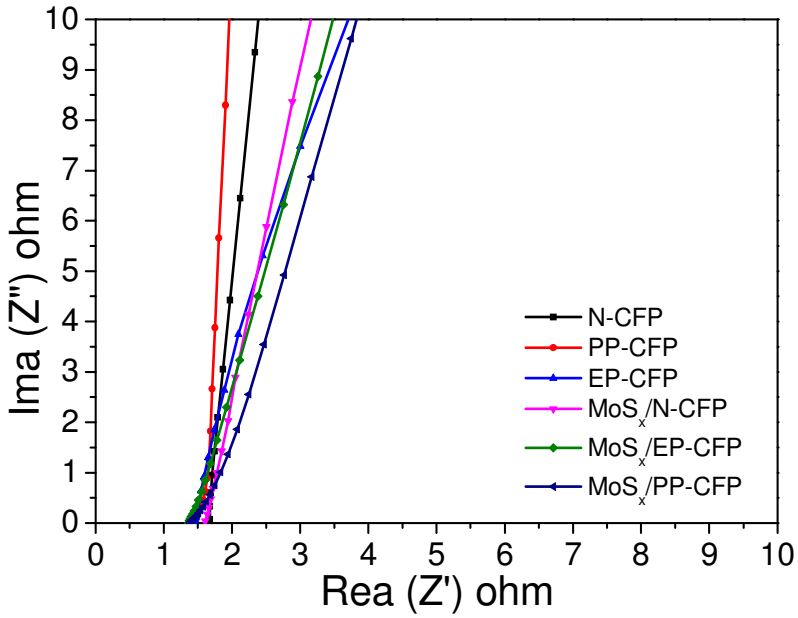

Figure S1. Series resistances of N-CFP, PP-CFP, EP-CFP, MoS_x/N-CFP, MoS_x/EP-CFP and MoS_x/PP-CFP.

Table S1. Series resistances of N-CFP, EP-CFP, PP-CFP, MoS_x/N-CFP, MoS_x/EP-CFP and MoS_x/PP-CFP

Samples	Series Resistance (Rs) (ohm)
N-CFP	1.76
EP-CFP	1.42
PP-CFP	1.45
MoS_x/N-CFP	1.56
MoS_x/EP-CFP	1.35
MoS_x/PP-CFP	1.37

The crystalline MoS_2 has a poor catalytic activity due to the large internal resistance, especially in the direction perpendicular to the MoS_2 layer. The electrical conductivity of crystalline MoS_2 is extremely anisotropic so that the conductivity (10^{-5} – 10^{-4} Ω^{-1} cm^{-1}) in the direction perpendicular to the MoS_2 layer is approximately 3 orders of magnitude smaller than that (10^{-2} – 10^{-1} Ω^{-1} cm^{-1}) parallel to the layer. However, according to our previous work published in Ref.41, amorphous molybdenum sulfide has a high conductivity (0.22 Ω^{-1} cm^{-1}) because of the defective and isotropic nature. In the specification table of the Toray CFP (TGP-H-120), the electrical resistivity of the CFP is 80 mΩcm in the perpendicular direction and 4.7 mΩcm in the parallel direction to the plane. These values correspond to the conductivity of 13~213 Ω^{-1} cm^{-1}. (see http://fuelcellstore.com/toray-carbon-paper-120). Even though the conductivity of the amorphous MoS_x is smaller than that of CFP, the conductivity of the amorphous phase is not so poor as the crystalline phase exhibits. As well known, the series resistance primarily comes from wiring and the electrolyte solution, while the resistance of MoS_x is negligible comparing to the others. In our experiments, the electrical wires were connected on CFPs with silver paste. Since the amount and the area of the silver paste applied were not precisely controlled to be identical for each sample, the main origin of the series resistance variation may be the wiring. However, the series resistances of all specimens are low enough to be used for the *iR* drop calculation.

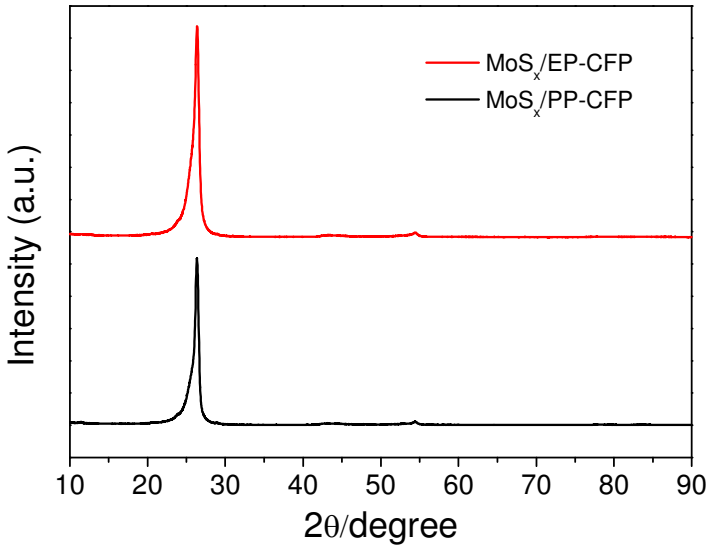

Figure S2. X-ray diffraction patterns of MoS_x/EP-CFP and MoS_x/PP-CFP. The peaks are originated from the crystalline graphite-like carbon.

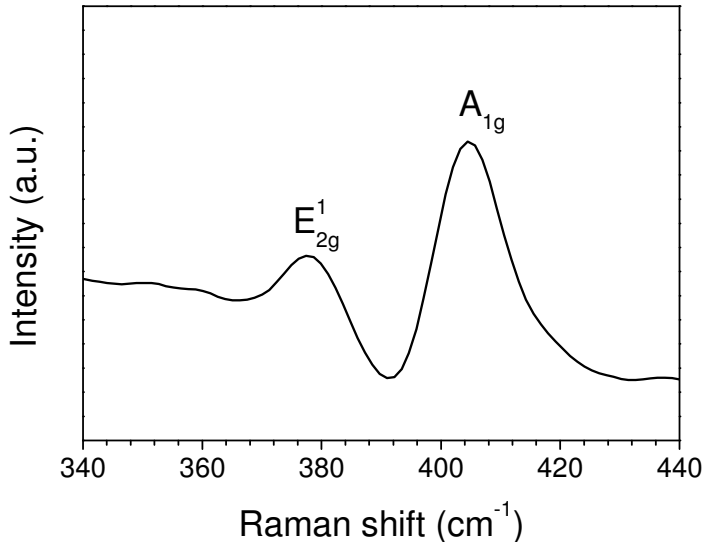

Figure S3. Raman spectrum of MoS_x/PP-CFP

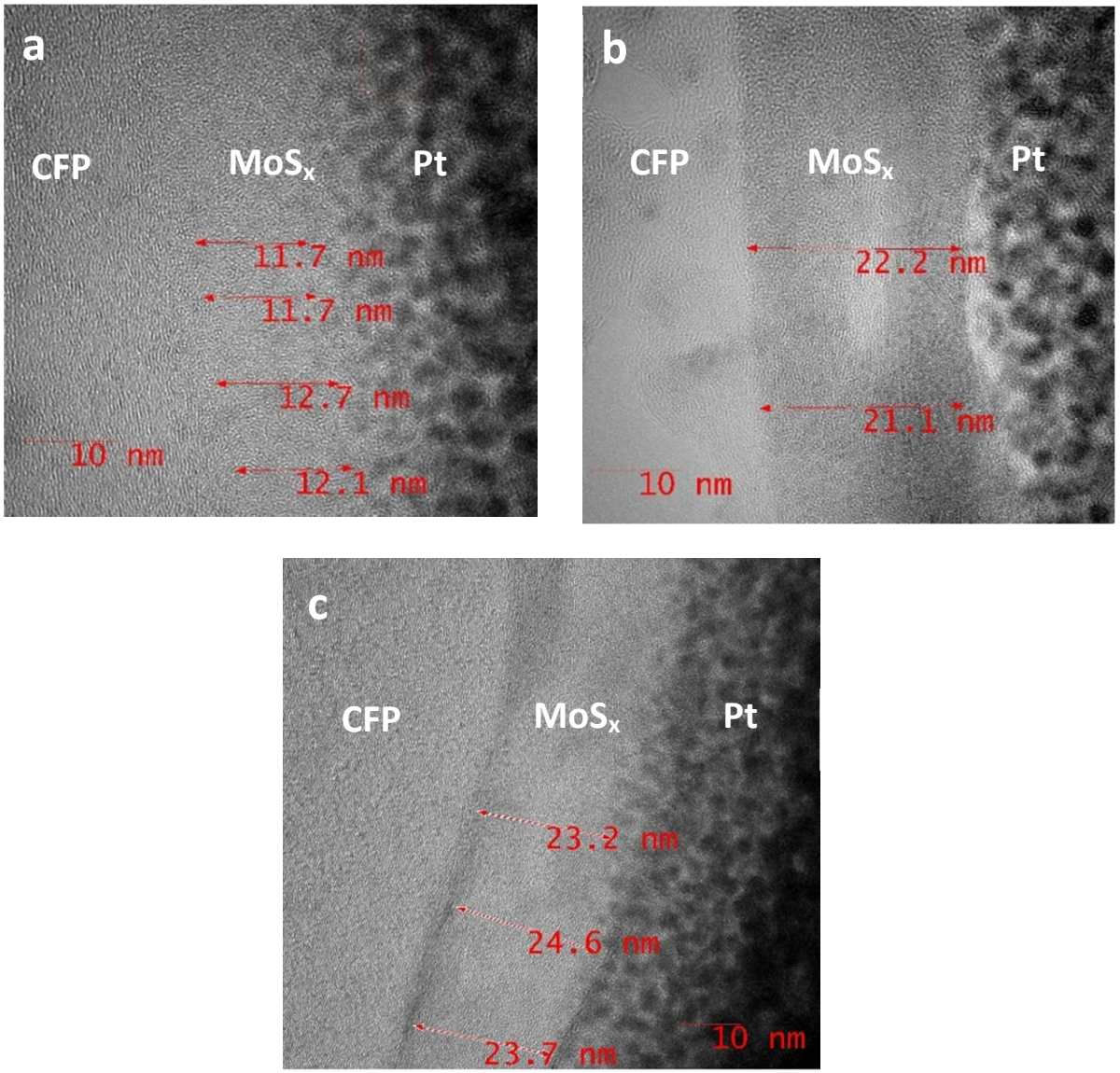

Figure S4. HR-TEM images (cross-sectional view) of (a) MoS_x/N-CFP, (b) MoS_x/PP-CFP, and (c) MoS_x/EP-CFP. The center part of each images show the thin layer of MoS_x.

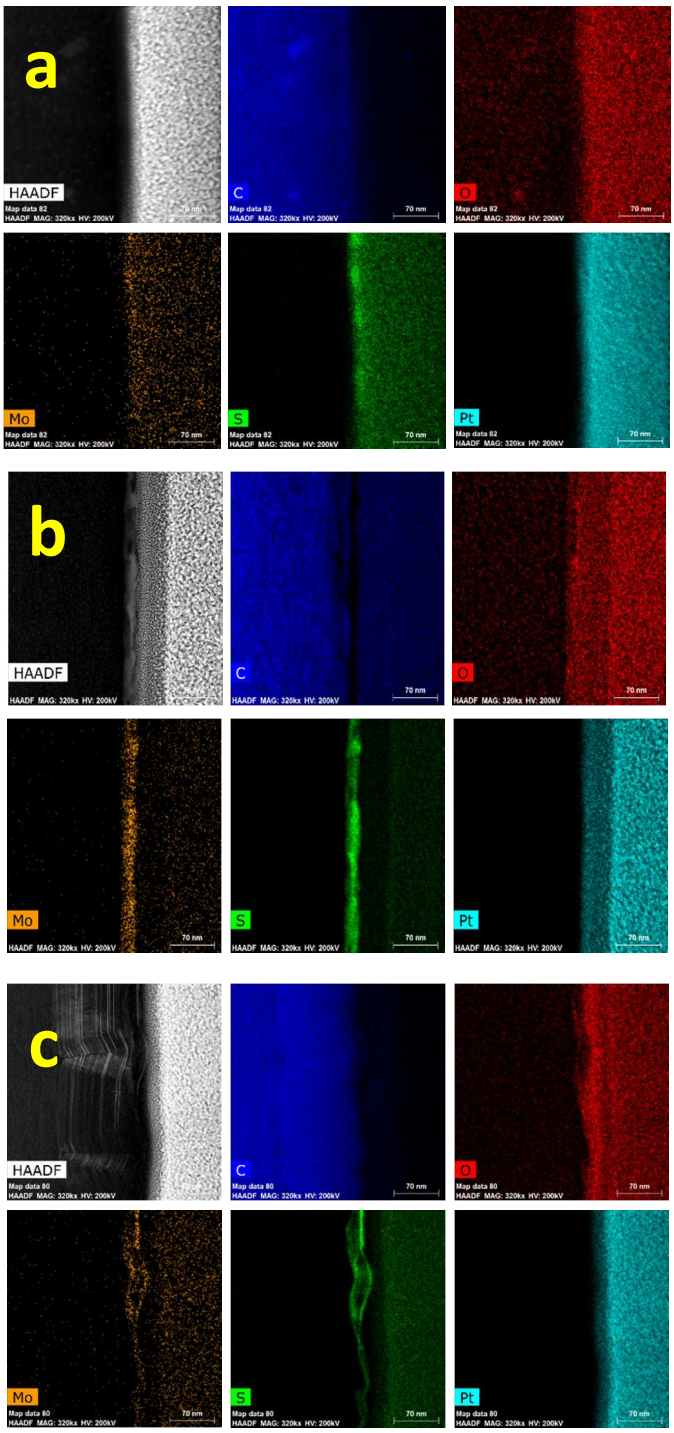

Figure S5. STEM images and elemental maps of (a) MoS_x/N-CFP, (b) MoS_x/PP-CFP, and (c) MoS_x/EP-CFP.

Table S2. Deconvoluted XPS data for various MoS_x samples.

Samples	Mo (eV)		S^{2-} (eV)		S_2^{2-} (eV)	
	$3d_{5/2}$	$3d_{3/2}$	$2p_{3/2}$	$2p_{1/2}$	$2p_{3/2}$	$2p_{1/2}$
MoS_x/N- CFP	229.1	232.3	161.4	162.6	162.8	164.0
MoS_x/ EP-CFP	229.2	232.3	161.9	163.0	163.3	164.5
MoS_x/ PP-CFP	229.2	232.4	161.5	162.7	162.9	164.1

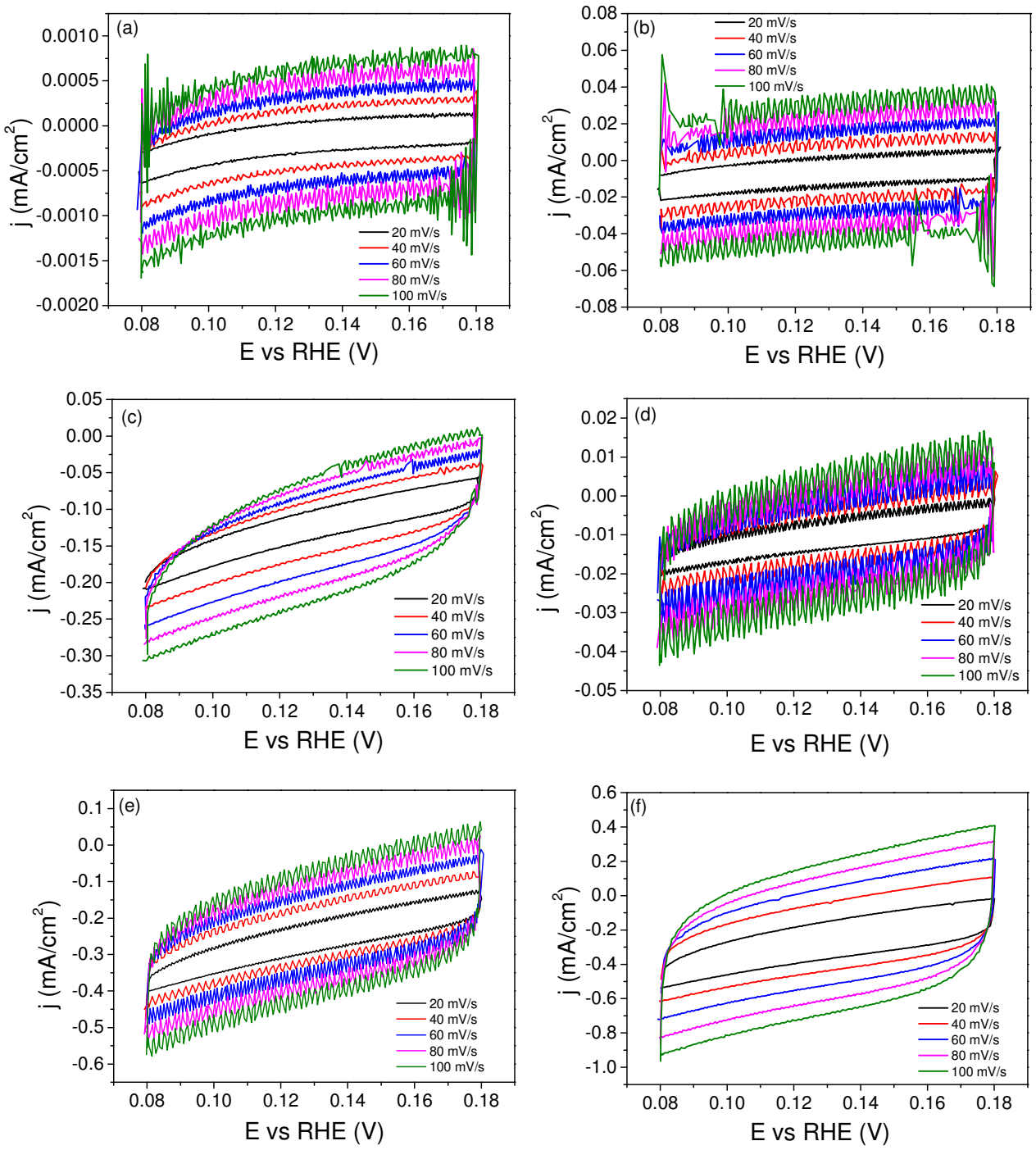

Figure S6. Electrochemical capacitance measurements for determination of surface area: (a) N-CFP, (b) PP-CFP, (c) EP-CFP, (d) MoS_x/N-CFP, (e) MoS_x/EP-CFP and (f) MoS_x/PP-CFP.

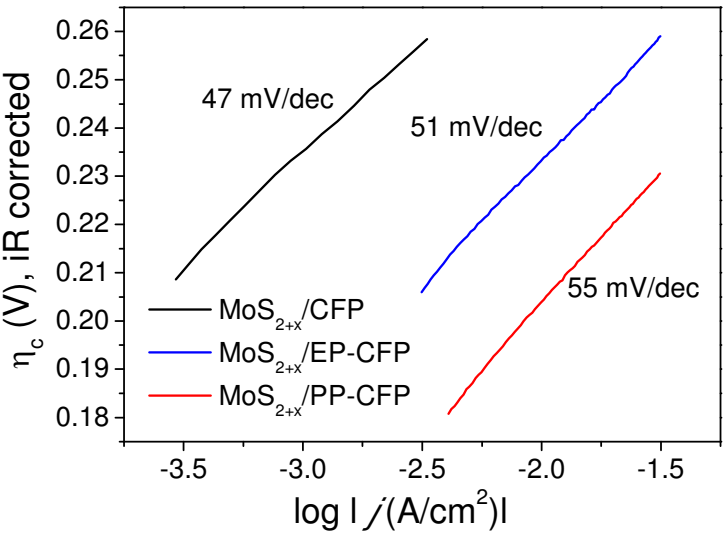

Figure S7. Tafel plots of MoS_x/N-CFP, MoS_x/EP-CFP and MoS_x/PP-CFP after 1000 cycles.